2023 IEEE 28th International Workshop on Computer Aided Modeling and Design of Communication Links and Networks (CAMAD)

2023 IEEE 28th International Workshop on Computer Aided Modeling and Design of Communication Links and Networks (CAMAD) | 979-8-3503-0349-0/23/$31.00 ©2023 IEEE | DOI: 10.1109/CAMAD59638.2023.10478402

Theoretical Limits of SoOP TDOA Localization of Unmanned Systems with Imperfect Synchronization

Khaled Walid Elgammal*, Berke Can Turan†, Oguz Bedir*, Hasari Celebi‡,
Marwa K. Qaraqe§, and Mehmet Kemal Ozdemir*
*School of Engineering and Natural Sciences, Istanbul Medipol University, Istanbul, Turkey
† Faculty of Engineering and Natural Sciences, Sivas University of Science and Technology, Sivas, Turkey
‡Department of Computer Engineering, Gebze Technical University, Kocaeli, Turkey
§College of Science and Engineering, Hamad Bin Khalifa University, Doha, Qatar
khaled.abdelfatah@std.medipol.edu.tr, berke.turan@sivas.edu.tr, oguz.bedir@std.medipol.edu.tr,
hcelebi@gtu.edu.tr, mqaraqe@hbku.edu.qa, and mkozdemir@medipol.edu.tr

***Abstract*—Self-localization is of crucial importance to Unmanned Aerial Vehicle (UAV) industry. Localization systems such as the Global Positioning System (GPS) are prone to jamming and spoofing. Localization using the Signal-Of-Opportunity (SoOP) gained much attention recently as an alternative to typical localization systems. We consider a general scenario where a receiver deployed on a mobile UAV finds its location based on Time Difference Of Arrival (TDOA) measurements with a number of unsynchronized reference Base Station (BS) receivers using signals from unsynchronized transmitters. The UAV has relative time offsets and clock skews with the BSs. We derive the Cramer-Rao Lower Bound (CRLB) of the UAV location and relative skews. Then, we plot them for Phase Alternating Line (PAL) analog TV transmission as SoOP.**

***Index Terms*—TDOA, signals of opportunity, SoOP, UAV, receiver self-localization, non-GPS, Line-Of-Sight, LOS**

I. Introduction

Self-localization is a primary requirement for UAV systems. Typically, a GPS receiver allows a UAV to find its location with high accuracy. However, the UAV GPS receiver needs to have Line-Of-Sight (LOS) with at least four GPS satellites [1]. GPS signals are not always available and are susceptible to jamming and spoofing [2]. A popular alternative is to use the SoOPs available in the surrounding area. SoOP-based localization uses measurements of Received Signal Strength (RSS) such as in [3], TDOA such as in [4], Time Of Arrival (TOA) such as in [5], Direction Of Arrival (DOA) such as in [6], or a hybrid combination of two or more of them [7]. TDOA measurements calculate the difference in TOA between two different receivers. A typical mobile receiver positioning system uses a single reference receiver and several signal transmission sources. Each source transmits a signal of opportunity, which both the mobile and the reference receivers receive. Since the receivers have no control over the SoOP transmitters and the transmission time of SoOPs is unknown to the receivers, the reference receiver provides a common time reference for all receivers. However, it is not easy to synchronize the clocks of the receivers with high accuracy, which results in relative clock skews and time offsets. Alternatively, differential TDOA removes the need for time synchronization but requires an additional hardware deployment such as in [8], [9], and [10]. However, differential TDOA studies propose various measurement schemes and algorithms. Every study applies a different geometric solution to find the position. [8] and [10] generate ellipsoids for the line of positions (LOP)s while [9] generates hyperbola for the LOPs.

Many studies discuss the TDOA-based algorithms and the theoretical limits for different localization scenarios, including the UAV self-localization [11]. However, no study considers the effect of the velocity of the UAV on the theoretical limits of the TDOA-based UAV self-localization when acting as a receiver. Motivated by this, we consider the problem of mobile UAV TDOA-based localization using the SoOP in the presence of relative clock offsets and skews with several reference BSs' receivers. We derive and plot the CRLB of the location of the UAV and the relative skews in the presence of Doppler frequency shift. The primary contribution of this work lies in deriving the CRLB for the moving UAV's location estimation and relative clock skews. This analysis provides a theoretical performance limit for the accuracy of the localization process in the considered scenario. Furthermore, the paper presents plots of the CRLB specifically for PAL analog TV transmission as the SoOP. The rest of the paper is organized as follows: in Section II, we develop the system model. In Section III, we derive the CRLB. Finally, we present the figures of the derived CRLB in Section IV.

II. Problem Statement

In our model, the SoOP is received by two or more separate stations. One station, the movingUAV, is at an unknown

The work of Hasari Celebi was supported by the Turkish Scientific and Research Council (TUBITAK) under Grant 120N573.

This publication was made possible by AICC03-0324-200005 from the Qatar National Research Fund (a member of Qatar Foundation). The findings herein reflect the work, and are solely the responsibility, of the authors.

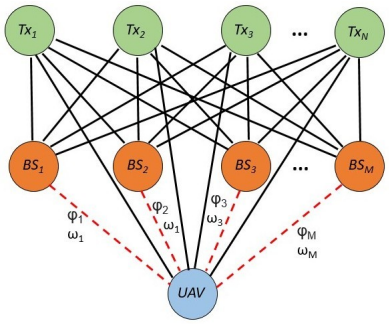

Fig. 1. Formulation of system equations.

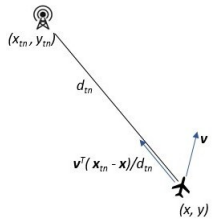

Fig. 2. UAV in motion (the z-direction is not shown).

location, while the rest, the BSs, are reference receivers at known locations. The SoOP transmitters Tx_N locations are assumed to be known. However, their transmission times are unknown, and their clocks are independent of each other and the receivers' clocks. Fixed SoOP transmitters' locations can be determined prior through surveying.

We assume that the UAV clock has an independent time offset and clock skew relative to each BS. Figure 1 represents the system equations where each black line corresponds to a signal transmitted from one of the SoOP broadcasters and received at the UAV or a BS. Each red line corresponds to a number of TDOAs parameterized by a relative clock offset and skew. As in [12], we assume that the relation between the clock of the mth BS, $t|_{b_m}$, and the clock of the UAV, $t|_u$, is

$$t|_u = \phi_m + \omega_m t|_{b_m}, \tag{1}$$

where ϕ_m and ω_m are the relative clock offset and the time-independent clock skew between the UAV and the mth BS, respectively. Additionally, we assume that the UAV preserves line-of-sight with the transmitters and moves with uniform velocity $\boldsymbol{v}$ as shown in Fig. 2. The velocity vector has a component in the direction of the nth transmitter, where the relative motion between the transmitter and the UAV exhibits a Doppler effect.

If the transmission time of the signal at the nth transmitter is T_{o_n} and c is the speed of light, then the noiseless measured TOA at the mth BS is

$$t_{nm} = T_{o_n} + d_{t_n b_m}/c, \tag{2}$$

where $d_{t_n b_m}$ is the distance between the nth transmitter and the mth BS given by

$$d_{t_n b_m} = \sqrt{(x_{t_n} - x_{b_m})^2 + (y_{t_n} - y_{b_m})^2 + (z_{t_n} - z_{b_m})^2}, \tag{3}$$

where $\boldsymbol{x_{t_n}} = [x_{t_n}\ y_{t_n}\ z_{t_n}]^T$ and $\boldsymbol{x_{b_m}} = [x_{b_m}\ y_{b_m}\ z_{b_m}]^T$ are the known transmitter and BS coordinates, respectively. The noiseless measured TOA at UAV of the signal from the nth transmitter relative to the mth receiving BS, t^u_{nm}, can be modeled as follows:

$$t^u_{nm} = \phi_m + \omega_m(T_{o_n} + d_{t_n}/c), \tag{4}$$

where d_{t_n} is the distance between the UAV and the nth transmitter, and is given by

$$d_{t_n} = \sqrt{(x - x_{t_n})^2 + (y - y_{t_n})^2 + (z - z_{t_n})^2} = \|(\boldsymbol{x_{t_n}} - \boldsymbol{x})\|, \tag{5}$$

where $\boldsymbol{x} = [x\ y\ z]^T$ are the coordinates of the UAV. Since the UAV is moving as shown in Fig. 2, the frequency of the received signal from the nth transmitter exhibits a doppler frequency shift:

$$\Delta f_n = \frac{f_n}{c}\frac{\boldsymbol{v}^T(\boldsymbol{x_{t_n}} - \boldsymbol{x})}{d_{t_n}}, \tag{6}$$

where f_n is the carrier frequency of the signal from the nth transmitter, and $\boldsymbol{v} = [v_x\ v_y\ v_z]^T$ is the velocity vector. Considering the relation between the carrier frequency of the nth transmitted signal, f_n, and that of the arriving signal, f'_n:

$$f'_n = f_n(1 + \frac{\boldsymbol{v^T}(\boldsymbol{x_{t_n}} - \boldsymbol{x})}{cd_{t_n}}). \tag{7}$$

The corresponding change in the signal period is:

$$\frac{1}{f'_n} = \frac{1}{f_n}(1 - \frac{\boldsymbol{v^T}(\boldsymbol{x_{t_n}} - \boldsymbol{x})}{cd_{t_n} + \boldsymbol{v^T}(\boldsymbol{x_{t_n}} - \boldsymbol{x})}). \tag{8}$$

The corresponding Doppler shift affecting the TOA:

$$\Delta TOA_n = -\frac{1}{f_n}\frac{\boldsymbol{v}^T(\boldsymbol{x_{t_n}} - \boldsymbol{x})}{cd_{t_n} + \boldsymbol{v}^T(\boldsymbol{x_{t_n}} - \boldsymbol{x})}. \tag{9}$$

This Doppler shift affects the TOA measurements as follows:

$$t^u_{nm} = \phi_m + \omega_m(T_{o_n} + d_{t_n}/c) - \frac{1}{f_n}\frac{\boldsymbol{v}^T(\boldsymbol{x_{t_n}} - \boldsymbol{x})}{cd_{t_n} + \boldsymbol{v}^T(\boldsymbol{x_{t_n}} - \boldsymbol{x})}. \tag{10}$$

The noisy measured TDOA between the UAV and the mth BS using the signal from the nth transmitter can be found by:

$$\delta_{nm} = t^u_{nm} - t_{nm} = \phi_m + \omega_m\left(T_{o_n} + \frac{d_{t_n}}{c}\right) - \frac{1}{f_n}\frac{s_n}{cd_{t_n} + s_n} - T_{o_n} - \frac{d_{t_n b_m}}{c} + \epsilon_{nm}, \tag{11}$$

where the measurement noise ϵ_{nm} is independent Additive White Gaussian Noise (AWGN), $\epsilon_{nm} \sim \mathcal{N}(0, \sigma^2_{nm})$, and $s_n = \boldsymbol{v}^T(\boldsymbol{x_{t_n}} - \boldsymbol{x})$.

III. CRLB Calculation

Let (x, y, z) be the coordinates of the UAV, then, the vector of unknown parameters is given as

$$\boldsymbol{\theta} = [x\ y\ z\ \omega_1\ ...\omega_M]^T \quad \in \mathbb{R}^{M+3} \tag{12}$$

We consider the transmission times as nuisance parameters that appear in the final CRLB. The vector form of the TDOAs between the UAV and the mth BS is as follows:

$$\boldsymbol{\delta_m} = [\delta_{1m}\ \delta_{2m}\ ...\ \delta_{Nm}]^T \in \mathbb{R}^N \tag{13}$$

All the TDOA measurements can be formulated as a single vector $\boldsymbol{\Delta}$ as follows:

$$\boldsymbol{\Delta} = \left[\boldsymbol{\delta_1}^T \ \ ... \ \ \boldsymbol{\delta_M}^T\right]^T \in \mathbb{R}^{N\times M} \tag{14}$$

The mean of the TDOA between the UAV and the mth reference receiver for the signal from the the nth transmitter is

$$\mu_{nm} = E[\delta_{nm}] = \phi_m + \omega_m\left(T_{o_n} + \frac{d_{t_n}}{c}\right) - \frac{1}{f_n}\frac{s_n}{cd_{t_n} + s_n} - T_{o_n} - \frac{d_{t_n b_m}}{c} \tag{15}$$

The mean vector of the TDOAs between the mth BS and the UAV for all transmitters is as follows:

$$\boldsymbol{\mu}_m = [E\{\delta_{1m}\} \ \ E\{\delta_{2m}\} \ \ ... \ \ E\{\delta_{Nm}\}]^T \in \mathbb{R}^N \tag{16}$$

The means of all TDOAs in a single vector can be written as:

$$\boldsymbol{\mu} = \left[\boldsymbol{\mu}_1^T \boldsymbol{\mu}_2^T ... \boldsymbol{\mu}_M^T\right]^T \in \mathbb{R}^{NM} \tag{17}$$

The covariance matrix for the TDOAs of the mth BS is:

$$\boldsymbol{C_m} = diag(\sigma_{1m}^2, \sigma_{2m}^2, ..., \sigma_{Nm}^2) \in \mathbb{R}^{N\times N} \tag{18}$$

where $diag$ is the diagonal matrix. Then, the covariance matrix of all TDOAs is:

$$\boldsymbol{C} = blkdiag(\boldsymbol{C_1}, \boldsymbol{C_2}, ..., \boldsymbol{C_M}). \tag{19}$$

The noise variance of the TDOA measurement is distance-dependent and can be modeled as a function of Signal-to-Noise Ratio (SNR) and bandwidth β such as in [13]:

$$\sigma_{nm}^2 = \frac{1}{\beta^2}\left(\frac{1}{SNR_n} + \frac{1}{SNR_{nm}}\right), \tag{20}$$

where SNR_n and SNR_{nm} are the SNR of the signal from the nth transmitter received at the UAV and the mth BS, respectively. The SNR at a receiving node is:

$$SNR = \frac{P_T}{P_n}\frac{1}{PL}, \tag{21}$$

where P_T, P_N, and PL are the transmitted power, thermal noise power, and the corresponding path loss, respectively. The free space path loss for isotropic antennae depends on the distance d between the transmitter and the receiver such that:

$$PL = \left(\frac{4\pi df}{c}\right)^2, \tag{22}$$

where f is the frequency carrier. The noise variance can then be defined as follows:

$$\sigma_{nm}^2 = \frac{1}{c^2}\frac{P_N}{P_T}\left(\frac{4\pi f}{\beta}\right)^2\left(d_{t_n}^2 + d_{t_n b_m}^2\right), \tag{23}$$

where $d_{t_n b_m}$ is the distance between the nth transmitter and the mth BS.

The element of the Fisher Information Matrix (FIM) located at the ith row and j column can be expressed as in [14]:

$$[\boldsymbol{I_\theta}]_{ij} = \left[\frac{\partial\boldsymbol{\mu}(\boldsymbol{\theta})}{\partial\theta_i}\right]^T \boldsymbol{C}^{-1}(\theta)\left[\frac{\partial\boldsymbol{\mu}(\boldsymbol{\theta})}{\partial\theta_j}\right] + \frac{1}{2}tr\left[\boldsymbol{C}^{-1}(\boldsymbol{\theta})\frac{\partial\boldsymbol{C}(\boldsymbol{\theta})}{\partial\theta_i}\boldsymbol{C}^{-1}(\boldsymbol{\theta})\frac{\partial\boldsymbol{C}(\boldsymbol{\theta})}{\partial\theta_j}\right]. \tag{24}$$

The derivative of the mean TDOA of nth transmitter and mth reference receiver with respect to x is:

$$\frac{\partial E\{\delta_{nm}\}}{\partial x} = \frac{\omega_m\Delta x_n}{cd_{t_n}} + \frac{c}{d_{t_n}f_n}\frac{s_n\Delta x_n + v_x d_{t_n}^2}{(cd_{t_n} + s_n)^2}, \tag{25}$$

where $\Delta x_n = (x - x_{t_n})$. The derivative of the mean TDOA of nth transmitter and mth reference receiver with respect to y is:

$$\frac{\partial E\{\delta_{nm}\}}{\partial y} = \frac{\omega_m\Delta y_n}{cd_{t_n}} + \frac{c}{d_{t_n}f_n}\frac{s_n\Delta y_n + v_y d_{t_n}^2}{(cd_{t_n} + s_n)^2}, \tag{26}$$

where $\Delta y_n = (y - y_{t_n})$. Similarly,

$$\frac{\partial E\{\delta_{nm}\}}{\partial z} = \frac{\omega_m\Delta z_n}{cd_{t_n}} + \frac{c}{d_{t_n}f_n}\frac{s_n\Delta z_n + v_z d_{t_n}^2}{(cd_{t_n} + s_n)^2}, \tag{27}$$

where $\Delta z_n = (z - z_{t_n})$. The derivative of the mean TDOA of nth transmitter and mth reference receiver with respect to ω_m is:

$$\frac{\partial E\{\delta_{nm}\}}{\partial\omega_m} = T_{o_n} + \frac{d_{t_n}}{c} \tag{28}$$

$$\frac{\partial\boldsymbol{\mu}}{\partial\omega_m} = \left[\mathbf{0}_{(m-1)N}^T \ \ \left[\frac{\partial\boldsymbol{\mu_m}}{\partial\omega_m}\right]^T \ \ \mathbf{0}_{(M-m)N}^T\right]^T, \tag{29}$$

where $\mathbf{0}_m$ is the zero vector of size m. The derivative of the variance with respect to x is:

$$\frac{\partial\sigma_{nm}^2}{\partial x} = \frac{2}{c^2}\frac{P_N}{P_T}\left(\frac{4\pi f}{\beta}\right)^2(\Delta x_n) = \frac{2\sigma_{nm}^2}{d_{t_n}^2 + d_{t_n b_m}^2}\Delta x_n. \tag{30}$$

The derivative of the variance with respect to y is:

$$\frac{\partial\sigma_{nm}^2}{\partial y} = \frac{2}{c^2}\frac{P_N}{P_T}\left(\frac{4\pi f}{\beta}\right)^2(\Delta y_n) = \frac{2\sigma_{nm}^2}{d_{t_n}^2 + d_{t_n b_m}^2}\Delta y_n. \tag{31}$$

Similarly,

$$\frac{\partial\sigma_{nm}^2}{\partial z} = \frac{2}{c^2}\frac{P_N}{P_T}\left(\frac{4\pi f}{\beta}\right)^2(\Delta z_n) = \frac{2\sigma_{nm}^2}{d_{t_n}^2 + d_{t_n b_m}^2}\Delta z_n. \tag{32}$$

The derivative of the variance with respect to ω_m is:

$$\frac{\partial\sigma_{nm}^2}{\partial\omega_m} = 0. \tag{33}$$

Assuming that the UAV maximum speed is 500Km/h, the TV transmission is using the UHF band, and the region of

operation has a radius lower than 50Km, then the elements of FIM can be approximated to:

$$[\boldsymbol{I_\theta}]_{11} = \sum_{m=1}^{M}\sum_{n=1}^{N}\Delta x_n^2\Big\{\frac{2}{(d_{t_n}^2+d_{t_nb_m}^2)^2}+ \frac{\omega_m^2}{c^2 d_{t_n}^2\sigma_{nm}^2}\big[1+2\frac{c^2}{\omega_m f_n}\frac{s_n\Delta x_n+v_x d_{t_n}^2}{(cd_{t_n}+s_n)^2\Delta x_n}\big]\Big\}. \quad (34)$$

$$[\boldsymbol{I_\theta}]_{22} = \sum_{m=1}^{M}\sum_{n=1}^{N}\Delta y_n^2\Big\{\frac{2}{(d_{t_n}^2+d_{t_nb_m}^2)^2}+ \frac{\omega_m^2}{c^2 d_{t_n}^2\sigma_{nm}^2}\big[1+2\frac{c^2}{\omega_m f_n}\frac{s_n\Delta y_n+v_y d_{t_n}^2}{(cd_{t_n}+s_n)^2\Delta y_n}\big]\Big\}. \quad (35)$$

$$[\boldsymbol{I_\theta}]_{33} = \sum_{m=1}^{M}\sum_{n=1}^{N}\Delta z_n^2\Big\{\frac{2}{(d_{t_n}^2+d_{t_nb_m}^2)^2}+ \frac{\omega_m^2}{c^2 d_{t_n}^2\sigma_{nm}^2}\big[1+2\frac{c^2}{\omega_m f_n}\frac{s_n\Delta z_n+v_z d_{t_n}^2}{(cd_{t_n}+s_n)^2\Delta z_n}\big]\Big\}. \quad (36)$$

$$[\boldsymbol{I_\theta}]_{44} = \sum_{n=1}^{N}\frac{1}{\sigma_{n1}^2}\left(T_{o_n}+\frac{d_{t_n}}{c}\right)^2. \quad (37)$$

$$[\boldsymbol{I_\theta}]_{12} = [\boldsymbol{I_\theta}]_{21} = \sum_{m=1}^{M}\sum_{n=1}^{N}\Delta x_n\Delta y_n\Bigg\{\frac{\omega_m}{\sigma_{nm}^2} \Big[\frac{\omega_m}{(cd_{t_n})^2}+\frac{1}{f_n(cd_{t_n}+s_n)^2}\left(\frac{2s_n}{d_{t_n}^2}+\frac{v_x}{\Delta x_n}+\frac{v_y}{\Delta y_n}\right)\Big]+ \frac{2}{(d_{t_n}^2+d_{t_nb_m}^2)^2}\Bigg\}. \quad (38)$$

$$[\boldsymbol{I_\theta}]_{13} = [\boldsymbol{I_\theta}]_{31} = \sum_{m=1}^{M}\sum_{n=1}^{N}\Delta x_n\Delta z_n\Bigg\{\frac{\omega_m}{\sigma_{nm}^2} \Big[\frac{\omega_m}{(cd_{t_n})^2}+\frac{1}{f_n(cd_{t_n}+s_n)^2}\left(\frac{2s_n}{d_{t_n}^2}+\frac{v_x}{\Delta x_n}+\frac{v_z}{\Delta z_n}\right)\Big]+ \frac{2}{(d_{t_n}^2+d_{t_nb_m}^2)^2}\Bigg\}. \quad (39)$$

$$[\boldsymbol{I_\theta}]_{23} = [\boldsymbol{I_\theta}]_{32} = \sum_{m=1}^{M}\sum_{n=1}^{N}\Delta y_n\Delta z_n\Bigg\{\frac{\omega_m}{\sigma_{nm}^2} \Big[\frac{\omega_m}{(cd_{t_n})^2}+\frac{1}{f_n(cd_{t_n}+s_n)^2}\left(\frac{2s_n}{d_{t_n}^2}+\frac{v_y}{\Delta y_n}+\frac{v_z}{\Delta z_n}\right)\Big]+ \frac{2}{(d_{t_n}^2+d_{t_nb_m}^2)^2}\Bigg\}. \quad (40)$$

$$[\boldsymbol{I_\theta}]_{14} = [\boldsymbol{I_\theta}]_{41} = \sum_{n=1}^{N}\frac{1}{\sigma_{n1}^2}\big(T_{o_n}+\frac{d_{t_n}}{c}\big) \big(\frac{\omega_1\Delta x_n}{cd_{t_n}}+\frac{c}{d_{t_n}f_n}\frac{s_n\Delta x_n+v_x d_{t_n}^2}{(cd_{t_n}+s_n)^2}\big). \quad (41)$$

$$[\boldsymbol{I_\theta}]_{24} = [\boldsymbol{I_\theta}]_{42} = \sum_{n=1}^{N}\frac{1}{\sigma_{n1}^2}\big(T_{o_n}+\frac{d_{t_n}}{c}\big) \big(\frac{\omega_1\Delta y_n}{cd_{t_n}}+\frac{c}{d_{t_n}f_n}\frac{s_n\Delta y_n+v_y d_{t_n}^2}{(cd_{t_n}+s_n)^2}\big). \quad (42)$$

$$[\boldsymbol{I_\theta}]_{34} = [\boldsymbol{I_\theta}]_{43} = \sum_{n=1}^{N}\frac{1}{\sigma_{n1}^2}\big(T_{o_n}+\frac{d_{t_n}}{c}\big) \big(\frac{\omega_1\Delta z_n}{cd_{t_n}}+\frac{c}{d_{t_n}f_n}\frac{s_n\Delta z_n+v_z d_{t_n}^2}{(cd_{t_n}+s_n)^2}\big). \quad (43)$$

This can be extended to any number of BSs with the conditions $i>3$ and $j>3$ as follows:

$$[\boldsymbol{I_\theta}]_{1i} = [\boldsymbol{I_\theta}]_{i1} = \sum_{n=1}^{N}\frac{1}{\sigma_{n(i-3)}^2}\big(T_{o_n}+\frac{d_{t_n}}{c}\big) \big(\frac{\omega_{i-2}\Delta x_n}{cd_{t_n}}+\frac{c}{d_{t_n}f_n}\frac{s_n\Delta x_n+v_x d_{t_n}^2}{(cd_{t_n}+s_n)^2}\big). \quad (44)$$

$$[\boldsymbol{I_\theta}]_{2i} = [\boldsymbol{I_\theta}]_{i2} = \sum_{n=1}^{N}\frac{1}{\sigma_{n(i-3)}^2}\big(T_{o_n}+\frac{d_{t_n}}{c}\big) \big(\frac{\omega_{i-2}\Delta y_n}{cd_{t_n}}+\frac{c}{d_{t_n}f_n}\frac{s_n\Delta y_n+v_y d_{t_n}^2}{(cd_{t_n}+s_n)^2}\big). \quad (45)$$

$$[\boldsymbol{I_\theta}]_{3i} = [\boldsymbol{I_\theta}]_{i3} = \sum_{n=1}^{N}\frac{1}{\sigma_{n(i-3)}^2}\big(T_{o_n}+\frac{d_{t_n}}{c}\big) \big(\frac{\omega_{i-3}\Delta z_n}{cd_{t_n}}+\frac{c}{d_{t_n}f_n}\frac{s_n\Delta z_n+v_z d_{t_n}^2}{(cd_{t_n}+s_n)^2}\big). \quad (46)$$

$$[\boldsymbol{I_\theta}]_{ij} = \begin{cases}\sum_{n=1}^{N}\frac{1}{\sigma_{(i-3)(j-3)}^2}\left(T_{o_n}+\frac{d_{t_n}}{c}\right)^2 & i=j\\ 0 & i\neq j\end{cases} \quad (47)$$

The FIM can be expressed in terms of its submatrices as follows:

$$\boldsymbol{I} = \begin{bmatrix}\boldsymbol{A} & \boldsymbol{B}\\ \boldsymbol{B}^T & \boldsymbol{D},\end{bmatrix}, \quad (48)$$

where

$$\boldsymbol{A} = \begin{bmatrix}[\boldsymbol{I_\theta}]_{11} & [\boldsymbol{I_\theta}]_{12} & [\boldsymbol{I_\theta}]_{13}\\ [\boldsymbol{I_\theta}]_{21} & [\boldsymbol{I_\theta}]_{22} & [\boldsymbol{I_\theta}]_{23}\\ [\boldsymbol{I_\theta}]_{31} & [\boldsymbol{I_\theta}]_{32} & [\boldsymbol{I_\theta}]_{33}\end{bmatrix},$$

$$\boldsymbol{B} = \begin{bmatrix}[\boldsymbol{I_\theta}]_{14} & .. & [\boldsymbol{I_\theta}]_{1(M+3)}\\ . & . & .\\ [\boldsymbol{I_\theta}]_{34} & .. & [\boldsymbol{I_\theta}]_{3(M+3)}\end{bmatrix},$$

$$\boldsymbol{D} = \begin{bmatrix}[\boldsymbol{I_\theta}]_{44} & ... & [\boldsymbol{I_\theta}]_{4(M+3))}\\ . & . & .\\ [\boldsymbol{I_\theta}]_{(M+3)4} & ... & [\boldsymbol{I_\theta}]_{(M+3)(M+3)}\end{bmatrix} \quad (49)$$

TABLE I
SIMULATION PARAMETERS OF ANALOG TV

β	8MHz
ω_m	1.0001
N	3
M	1
v	500Km/h
f_1, f_2, f_3	470MHz, 478MHz, 486MHz
P_T	$150KW \approx 81.76dBm$

The inverse of this matrix can be found as in [14]:

$$\left[\boldsymbol{I_\theta^{-1}}\right]_{\mathbf{11}} = (\boldsymbol{A} - \boldsymbol{B}\boldsymbol{D}^{-1}\boldsymbol{B}^T)^{-1} \quad (50)$$

$$\left[\boldsymbol{I_\theta^{-1}}\right]_{\mathbf{12}} = -(\boldsymbol{A} - \boldsymbol{B}\boldsymbol{D}^{-1}\boldsymbol{B}^T)^{-1}\boldsymbol{B}\boldsymbol{D}^{-1} \quad (51)$$

$$\left[\boldsymbol{I_\theta^{-1}}\right]_{\mathbf{21}} = -(\boldsymbol{D} - \boldsymbol{B}^T\boldsymbol{A}^{-1}\boldsymbol{B})^{-1}\boldsymbol{B}^T\boldsymbol{A}^{-1} \quad (52)$$

$$\left[\boldsymbol{I_\theta^{-1}}\right]_{\mathbf{22}} = (\boldsymbol{D} - \boldsymbol{B}^T\boldsymbol{A}^{-1}\boldsymbol{B})^{-1} \quad (53)$$

IV. CRLB FIGURES

We apply the derived CRLBs on the analog PAL TV signal. We show the position of each node alongside its number on the map (z-direction is removed for the sake of clarity). Then, we show the CRLB for different values of transmission parameters such as the SNR at the UAV and the BS, the bandwidth, the velocity, the number of transmitters, and the number of BSs. The generated map for the TV signal is shown in Fig. 3. The simulation parameters are as shown in Table I. The CRLB of the UAV estimated position and its relative skew for different values of SNR at UAV and BS is as shown in Figs. 4 and 5, respectively. The figures indicate that having an acceptable SNR at both receivers can attain better performance than having a high SNR at one receiver and a low SNR at the other. The dependence of CRLBs on the signal bandwidth, and UAV velocity is as shown in Figs. 6 and 7. The effect of velocity on the CRLBs is minor compared to the effect of the bandwidth. This is due to the practical limited speed range used in the simulation. The effect of the number of transmitters N and the number of BSs on the CRLBs is as shown in Figs. 8 and 9. Using $N = 5$ and $M = 3$ can achieve almost the minimum localization variance. Increasing M and N decreases the attainable variance marginally.

V. CONCLUSION

We considered the problem of UAV TDOA-based self-localization with the help of reference receiver(s). We derived and plotted the CRLB of the 2-dimensional position and the relative clock skew of the UAV with imperfect or no time synchronization. The achieved results agree with previous studies where lower CRLBs are attained using higher SNR, larger bandwidth, more SoOPs, and more reference BSs. It is found that the effect of the UAV velocity is minor on the position and the skew estimation. The attained CRLBs can be applied to different transmission types as long as a frame structure exists.

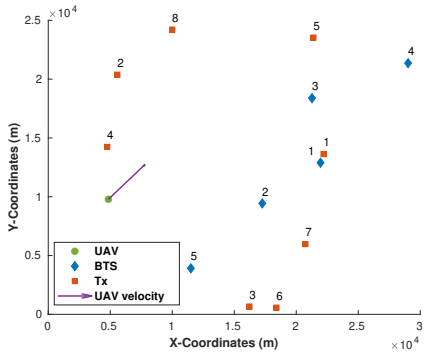

Fig. 3. Scenario map for PAL TV signal (velocity vector not to scale).

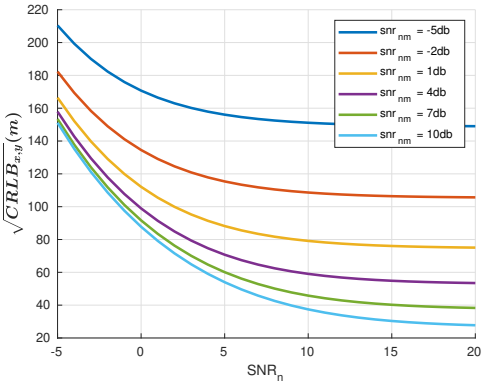

Fig. 4. The effects of the SNR on the position estimation.

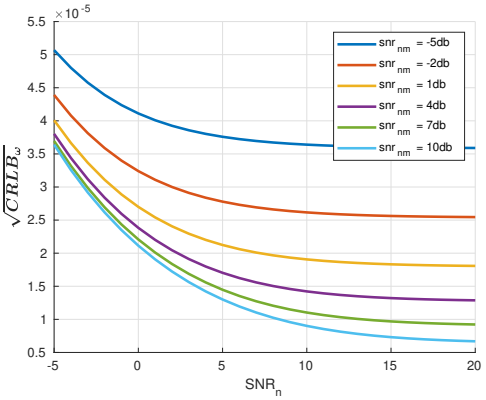

Fig. 5. The effects of the SNR on the skew estimation.

REFERENCES

[1] M. Nomura, T. Tanaka, and M. Yonekawa, "Gps positioning method under condition of only three acquired satellites," in *2008 SICE Annual Conference*, 2008, pp. 3487–3490.

[2] M. Cuntz, A. Konovaltsev, A. Dreher, and M. Meurer, "Jamming and spoofing in gps/gnss based applications and services – threats and countermeasures," in *Future Security*, N. Aschenbruck, P. Martini, M. Meier, and J. Tölle, Eds. Berlin, Heidelberg: Springer Berlin Heidelberg, 2012, pp. 196–199.

[3] M. Z. Karakusak, H. Kivrak, H. F. Ates, and M. K. Ozdemir, "Rss-based wireless lan indoor localization and tracking using deep architectures," *Big Data and Cognitive Computing*, vol. 6, no. 3, 2022. [Online]. Available: https://www.mdpi.com/2504-2289/6/3/84

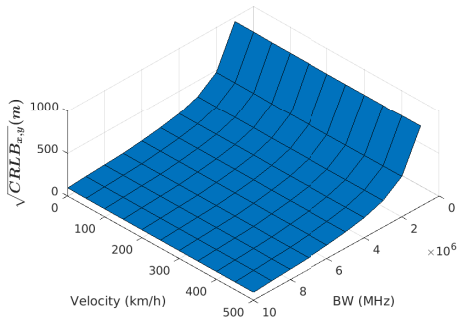

Fig. 6. The effects of the bandwidth and velocity on the position estimation.

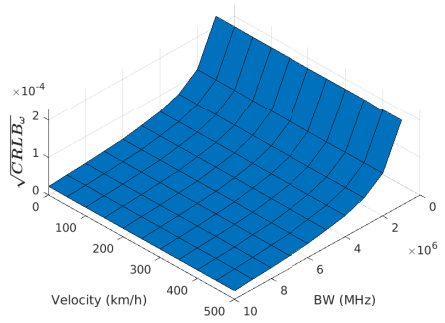

Fig. 7. The effects of the bandwidth and velocity on the skew estimation.

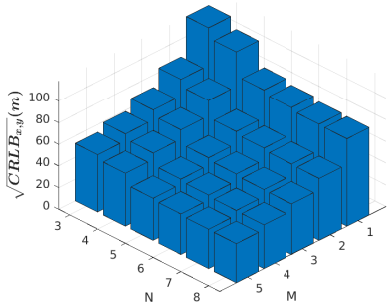

Fig. 8. The effects of N and M on the position estimation.

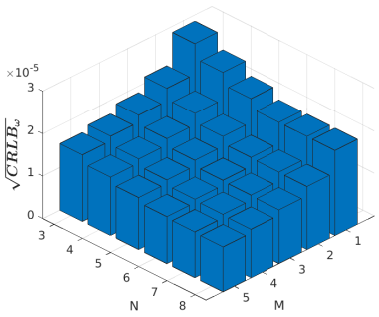

Fig. 9. The effects of N and M on the skew estimation.

[4] C. Yan and H. Howard Fan, "Asynchronous differential tdoa for non-gps navigation using signals of opportunity," in *2008 IEEE International Conference on Acoustics, Speech and Signal Processing*, 2008, pp. 5312–5315.

[5] H. Celebi and H. Arslan, "Adaptive positioning systems for cognitive radios," in *2007 2nd IEEE International Symposium on New Frontiers in Dynamic Spectrum Access Networks*, 2007, pp. 78–84.

[6] G. A. Fokin and I. V. Grishin, "Direction of arrival positioning requirements for location-aware beamforming in 5g mmwave udn," in *2022 Wave Electronics and its Application in Information and Telecommunication Systems (WECONF)*, 2022, pp. 1–6.

[7] N. Saeed, H. Nam, T. Y. Al-Naffouri, and M.-S. Alouini, "A state-of-the-art survey on multidimensional scaling-based localization techniques," *IEEE Communications Surveys Tutorials*, vol. 21, no. 4, pp. 3565–3583, 2019.

[8] S. He, X. Dong, and W.-S. Lu, "Localization algorithms for asynchronous time difference of arrival positioning systems," *EURASIP Journal on Wireless Communications and Networking*, vol. 2017, no. 9, pp. 1687–1499, 2017.

[9] K. W. Elgammal, B. C. Turan, O. Bedir, H. Celebi, and M. K. Ozdemir, "Signal of opportunity based TDOA positioning using analog TV signals," in *2023 Fourteenth International Conference on Ubiquitous and Future Networks (ICUFN) (ICUFN 2023)*, Paris, France, Jul. 2023, p. 4.

[10] M. Leng, W. P. Tay, C. M. S. See, S. Gulam Razul, and M. Z. Win, "Modified crlb for cooperative geolocation of two devices using signals of opportunity," *IEEE Transactions on Wireless Communications*, vol. 13, no. 7, pp. 3636–3649, 2014.

[11] A. Tahat, G. Kaddoum, S. Yousefi, S. Valaee, and F. Gagnon, "A look at the recent wireless positioning techniques with a focus on algorithms for moving receivers," *IEEE Access*, vol. 4, pp. 6652–6680, 2016.

[12] M. R. Gholami, S. Gezici, and E. G. Strom, "Tdoa based positioning in the presence of unknown clock skew," *IEEE Transactions on Communications*, vol. 61, no. 6, pp. 2522–2534, 2013.

[13] R. Álvarez, J. Díez-González, E. Alonso, L. Fernández-Robles, M. Castejón-Limas, and H. Perez, "Accuracy analysis in sensor networks for asynchronous positioning methods," *Sensors*, vol. 19, no. 13, 2019. [Online]. Available: https://www.mdpi.com/1424-8220/19/13/3024

[14] S. M. Kay, *Fundamentals of Statistical Signal Processing: Estimation Theory*. Pearson Education, 2013.